Fiber bundle model under fluid pressure

David Amitrano*
Université Grenoble Alpes, ISTerre, F-38000 Grenoble, France

Lucas Girard†
School of Architecture, Civil and Environmental Engineering, Ecole Polytechnique Fédérale de Lausanne, EPFL ENAC IIE CRYOS, Lausanne, Switzerland

(Received 26 August 2015; published 7 March 2016)

Internal fluid pressure often plays an important role in the rupture of brittle materials. This is a major concern for many engineering applications and for natural hazards. More specifically, the mechanisms through which fluid pressure, applied at a microscale, can enhance the failure at a macroscale and accelerate damage dynamics leading to failure remains unclear. Here we revisit the fiber bundle model by accounting for the effect of fluid under pressure that contributes to the global load supported by the fiber bundle. Fluid pressure is applied on the broken fibers, following Biot's theory. The statistical properties of damage avalanches and their evolution toward macrofailure are analyzed for a wide range of fluid pressures. The macroscopic strength of the new model appears to be strongly controlled by the action of the fluid, particularly when the fluid pressure becomes comparable with the fiber strength. The behavior remains consistent with continuous transition, i.e., second order, including for large pressure. The main change concerns the damage acceleration toward the failure that is well modeled by the concept of *sweeping of an instability*. When pressure is increased, the exponent β characterizing the power-law distribution avalanche sizes significantly decreases and the exponent γ characterizing the cutoff divergence when failure is approached significantly increases. This proves that fluid pressure plays a key role in failure process acting as destabilization factor. This indicates that macrofailure occurs more readily under fluid pressure, with a behavior that becomes progressively unstable as fluid pressure increases. This may have considerable consequences on our ability to forecast failure when fluid pressure is acting.

DOI: 10.1103/PhysRevE.93.033003

I. INTRODUCTION

The rupture of brittle materials is of major concern for many engineering applications and for geomaterials in the context of natural hazards. There is an important need to understand the evolution of mechanical properties in the vicinity of macrofailure in order to identify forerunners and to progress towards the prediction of failure (e.g., earthquakes [1], landslides [2], cliff collapse [3], etc.). In many cases, in both industrial and natural contexts, the progressive damage developed in presence of fluids can influence the rupture by modifying the stress state [e.g., Refs. 1–3]. The effect of fluid pressure on the stress state is generally assessed through the concept of effective pressure related to Biot's theory [4]:

$$\sigma' = \sigma + bp, \tag{1}$$

where σ' is the effective stress undergone by the bulk material, σ is the total stress, p is the fluid pressure, and b is Biot's coefficient. A part of the fluid pressure, formalized by the b coefficient, is transmitted to the bulk material. This parameter represents the sensitivity of the stress to the fluid pressure. Connectivity is assumed to be sufficiently large to allow fluid to be present anywhere in the medium. The physical interpretation of Biot's coefficient is the fraction of a surface on which the fluid pressure is applied. In the case of material partially broken, an analogy can be made between Biot's coefficient and the damage parameter, D, defined as the proportion of broken surface within the bulk material [5]:

$$D = \frac{S}{S_0}, \tag{2}$$

where S is the surface of the broken part of a section cut into the bulk and S_0 is the total surface, or the initial surface of the undamaged material. Biot's theory [4] is often used for analyzing the stress change induced by changes of water pressure in the case of fluid-induced seismicity, for landslides triggered by rainfall, and for geotechnical applications when the material is loaded in presence of fluids [6]. Many previous works considered a constant value of Biot's coefficient, generally near or equal to 1 (e.g., Refs. [1,2]). Such constant high values are reasonable when considering granular materials as natural soils or fault gouges for which the solid contact area is negligible compared with the area in contact with the fluid and does not significantly change during the deformation.

Contrastingly, for a material undergoing damage, as deformed brittle rocks or fibrous material, the b parameter should be considered as evolving. By analogy with the damage parameter, we suggest that, upon increasing load applied to the material, Biot's coefficient evolves from $b = 0$ for an intact material to $b = 1$ for a fully broken material. While several studies on progressive failure account for the evolution of damage as approaching failure [7–9], the link with the evolution of Biot's coefficient has not been considered yet. This is problematic because the sensitivity of stress to fluid pressure is likely to evolve when damage increases. Neglecting this evolution does not correctly reflect the role of fluid pressure on material progressive damage accumulation. In order to

*david.amitrano@univ-grenoble-alpes.fr
†lucas.girard@gmail.com

correctly account for this mechanism one may consider that any broken surface of the material contributes to supporting fluid pressure.

We propose a model that explicitly takes into account the link between damage and Biot's coefficient b and the damage parameter D considering simply $b = D$. The fiber bundle model (FBM) [10] is a good candidate for such an application as it explicitly expresses the proportion of broken fibers, i.e., the damage level, and the fact that this proportion increases when the applied load is increased.

Previous studies based on the FBM under force controlled loading and equal load sharing (ELS), have reported the following results (for an extended review see, e.g., Refs. [9,11]):

(1) Considering fiber strength spread at random from a uniform distribution between 0 and 1, macrofailure occurs at $\sigma_c = 0.25$ and $\epsilon_c = 0.5$, for a normalized Young's modulus, where σ_c and ϵ_c are the macroscopic stress and strain at failure, respectively.

(2) The avalanche size s, defined as the number of fibers failing during a loading step, is power-law distributed, $P(s) \sim s^{-\beta}$, with $\beta = 5/2$ for the complete set of avalanches. For a subset of avalanches occurring close to the macrofailure, avalanche sizes are also power-law distributed, with a lower exponent value, $P(s) \sim s^{-\tau}$, with $\tau = 3/2$.

(3) The susceptibility χ, defined as the number of fibers failing due to an infinitesimal change of the external stress (σ), $\chi = \delta \Sigma s / \delta \sigma$, follows a power-law divergence with the applied stress $\chi \sim (\sigma_c - \sigma)^{-1/2}$.

The same behavior is observed for the relaxation time T, which is the number of stress redistributions that the bundle takes to come to a stable fixed point at an external stress $\sigma, T \sim (\sigma_c - \sigma)^{-1/2}$.

(4) At the critical stress value σ_c, a fiber bundle shows a phase transition from a partially to a completely broken state. Different arguments have been proposed to establish the order of this phase transition [[11], p. 508]. For fiber bundles with global sharing rule, the proportion of surviving fiber, U, has been used to define the order parameter O [12]:

$$O = U(\sigma) - U(\sigma_c) \tag{3}$$

near the failure, $O \sim (\sigma_c - \sigma)^{1/2}$, showing a continuous transition from 1 to 0.

This transition can be alternatively analyzed by considering the branching ratio ζ [13,14]. ζ represents the probability to trigger future breaking events given an initial individual failure and is related to the number of broken fibers by

$$\zeta = 1 - \frac{1}{\langle s \rangle}, \tag{4}$$

$\langle s \rangle$ being the mean avalanche size. ζ continuously approaches the value 1 at the critical stress σ_c starting from zero for very small σ. It also shows a power-law trend, $(1 - \zeta) \sim (\sigma_c - \sigma)^{1/2}$. Therefore $(1 - \zeta)$ acts as an order parameter, showing a continuous transition at the critical point, signaling a second order phase transition [13].

In the present work, the effect of fluid pressure is accounted for by considering that fluid pressure is applied on each broken fiber, of unitary surface area, whereas the total load is sustained by the surviving (unbroken) fibers. The broken fibers represent the porosity of the material, which increases as damage progresses and through which the fluid pressure is applied to the solid skeleton. The fluid is supposed to be present everywhere, between the fibers, so that fluid pressure may be applied on any fiber without need of connectivity and independently from the damage state. This is a common hypothesis made in Biot's theory.

The paper is organized as follow. We first describe the change we make on the FBM to include the effect of fluid pressure. This new model is called fiber bundle model pressure (FBMP). Then the analysis of the statistical properties of bound breaking avalanches in the presence of pressured fluid is performed with particular focus on the evolution of these properties in the vicinity of failure and for a range of fluid pressures. This behavior is compared with the *dry* FBM, i.e., the original model without fluid pressure. The implications for the predictability of failure in the presence of fluid pressure are discussed.

II. METHOD

We consider the basic hypothesis that within a fiber bundle, the broken fibers represent the porosity of the damaged material on which the fluid pressure is applied. No fluid flow is considered, i.e., only static fluid pressure is accounted for. The fluid is considered to be present everywhere, between the fibers, so that fluid pressure may be applied on any fiber without need of connectivity between broken fibers. This is a common hypothesis made in Biot's theory. Accordingly, the FBM is modified to include the effect of fluid pressure on the broken fibers.

This needs to consider the section of the fibers, a, in order to calculate the force resulting from pressure applied. The total force, F_T, supported by the bundle is calculated as the sum of an external load, F_{ext}, and the load resulting from the fluid pressure applied on broken fibers, F_{fluid}:

$$F_T = F_{\text{ext}} + F_{\text{fluid}}, \tag{5}$$

$$F_{\text{fluid}} = p a n_b, \tag{6}$$

where p is the fluid pressure, n_b the number of broken fibers. It should be noted here that the usual FBM is recovered when p is set to zero. Considering the proportion of surviving fibers, $U = n_s/N$, where n_s is the number of surviving fibers and N is the total number of fibers, $n_s = N - n_b$.

The impact of the pressure on stress and strain can be demonstrated using a similar analysis as the dry FBM (e.g., Ref. [10]). The stress undergone by the each unbroken fiber is calculated considering the global shared load rules:

$$\sigma_{\text{fiber}} = \frac{F_T}{a n_s}. \tag{7}$$

In the following, a is set to unity for convenience:

$$\sigma_{\text{fiber}} = \frac{F_T}{NU} = \frac{F_{\text{ext}}}{NU} + \frac{p(1-U)N}{NU}. \tag{8}$$

Here we consider fiber strength randomly drawn from a uniform distribution ranging from 0 to 1. Consequently,

$$\sigma_{\text{fiber}} = 1 - U. \tag{9}$$

Equations (8) and (9) lead to

$$U = 1 - \frac{\sigma}{U} - p\frac{(1-U)}{U}, \tag{10}$$

where σ is the stress at macroscopic scale,

$$\sigma = \frac{F_{\text{ext}}}{N}. \tag{11}$$

The strain of the whole bundle is similar to that of individual fibers, since fibers are parallel and oriented in the direction of loading,

$$\epsilon = \frac{\sigma_{\text{fiber}}}{Y}, \tag{12}$$

Y being the Young's modulus, set to unity for convenience. So

$$\epsilon = 1 - U. \tag{13}$$

Equation (9) takes a quadratic form:

$$U^2 - U(1+p) + \sigma + p = 0. \tag{14}$$

The physically meaningful solution to this equation is

$$U = \frac{1+p}{2} + \sqrt{\frac{1}{4}(1-p)^2 - \sigma}, \tag{15}$$

$$U = \frac{1+p}{2} + \sqrt{\sigma_c - \sigma}, \tag{16}$$

with

$$\sigma_c = \tfrac{1}{4}(1-p)^2, \tag{17}$$

σ_c being the stress at failure. As a consequence, the strain at failure, ϵ_c, is

$$\epsilon_c = \tfrac{1}{2}(1-p). \tag{18}$$

This analysis shows that p strongly influences both stress and strain at failure. To examine properties of fiber failure avalanches for various p we performed numerical simulations. The loading is performed by progressively increasing the stress applied on the fibers. Each time the stress reaches the strength of a fiber (the weakest one), the fiber is broken, and n_s,n_b, and U are updated accordingly. The external force is kept constant to simulate stress-controlled loading. The stress on the remaining fibers is recalculated according to Eq. (7). The damage, D, corresponding to the proportion of broken fibers, $D = n_b/N = 1 - U$, is considered to be equal to Biot's coefficient, b. Since the number of unbroken fibers decreases and F_{ext} is kept constant after each rupture, the stress on the remaining fibers increases and some of them may reach their rupture point and eventually initiate an avalanches of ruptures. After each rupture, the stress on the remaining fibers is recalculated and the fibers reaching their strength are removed until the system recovers the stability; i.e., all the fibers are below their strength. The avalanche size, s, is considered to be the number of broken fibers during the whole avalanche. The number of iterations to recover the global stability is considered to represent the duration of the avalanche. Note that as the fluid pressure is kept constant and the number of broken fibers increases during an avalanche the load induced by the fluid also increases. This feature is the essential particularity of the model developed and is likely to promote the instability of the bundle when coming close to macrofailure. To examine this, we analyzed the behavior of systems with various pressure values. In order to scale the pressure with respect to the strength of the fibers we considered p ranging from 0 to 0.95, i.e., close to the maximal value of individual strength. The case $p = 1$ is clearly the limit of the previous analysis. Such a large p value leads to a highly unstable rupture associated with a few avalanches including almost all the fibers.

III. RESULTS

The results presented here correspond to $N = 10^6$ and p ranging from 0 to 0.95. Each configuration has been repeated several times in order to reach a good statistical representativity. As the number of broken fibers at failure decreases when p is increased, according to Eq. (13), we scaled the number of simulations by the factor $1/(1-p)$. So the number of simulations was $10^2(1-p)$ ranging from 100, for $p = 0$, to 2.10^4, for $p = 0.95$.

Here we report the main observations regarding the role of p on the behavior of the FBMP. We first verified that all

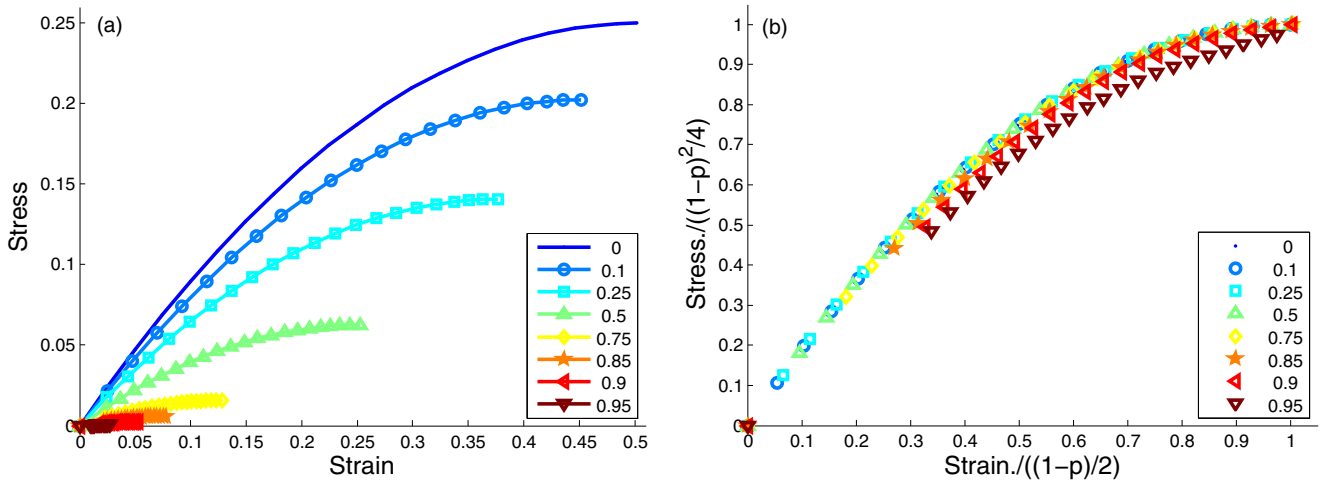

FIG. 1. (a) Stress versus strain for fluid pressure ranging from 0 to 0.95. (b) Stress versus strain normalized according to Eqs. (17) and (18).

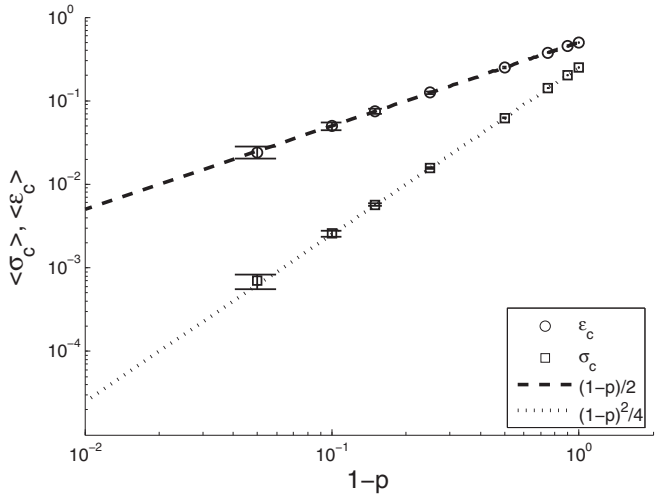

FIG. 2. Critical values of strain (ϵ_c) and stress (σ_c) at failure for fluid pressure p ranging from 0 to 0.95. Dotted lines corresponds to $0.5(1-p)$ and to $0.25(1-p)^2$ that analytically explain the pressure dependence of ϵ_c and σ_c, respectively.

the usual properties of the FBM summarized in Sec. I are recovered when p is set to zero.

The first notable impact of applying a fluid pressure on the FBM concerns the macroscopic behavior (strain-stress relation). Both stress and strain are strongly modified by the fluid pressure in accordance with Biot's theory (Fig. 1). The stress and strain value at the maximal strength are dramatically reduced when an increasing fluid pressure is applied. The reduction of strain and of the number of broken fibers are well captured by the scaling factor $\frac{1}{2}(1-p)$ while the stress decrease scales with $\frac{1}{4}(1-p)^2$ (Fig. 2) according to Eqs. (17) and (18).

The avalanche size distribution including all the damage events occurring during the simulation, pdf(s), is well defined by a power law, pdf(s) $\sim s^{-\beta}$ (Fig. 3) with a gradual decrease

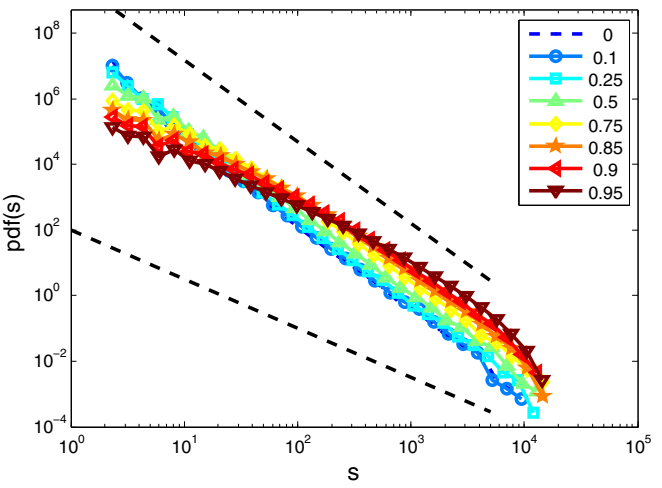

FIG. 3. Probability density function of the avalanche size, pdf(s), including all the rupture events, for fluid pressure p ranging from 0 to 0.95 (indicated in the legend). Dotted lines correspond to power-law exponents of -2.5 and -1.5, respectively.

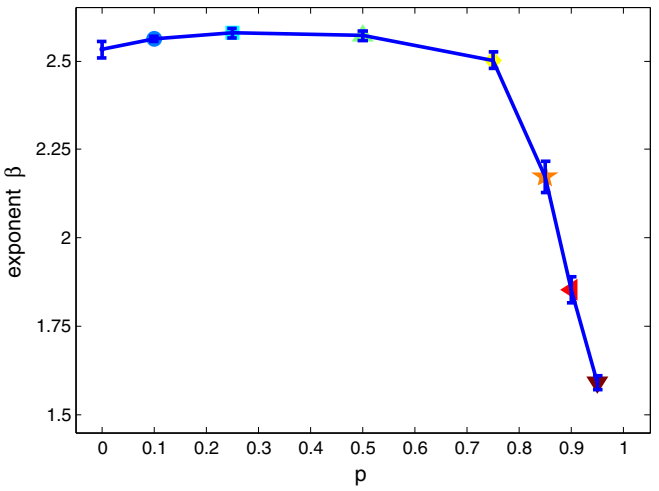

FIG. 4. Exponent β characterizing the pdf of the avalanche size for fluid pressure p ranging from 0 to 0.95 (indicated in the legend).

of the exponent β from 2.5 to 1.5 (Fig. 4) when pressure p becomes close to 1.

In order to examine the size distribution of avalanches occurring very close to the failure, we selected events with $\Delta = \sigma_C - \sigma < 10^{-4}$. Their size distribution obeys a power law, pdf$(s)_{\Delta\to 0} \sim s^{-\tau}$, with an exponent τ close to 1.5 which is independent of p (Fig. 5). This is a common feature of the dry FBM, which indicates that the fluid pressure does not affect the distribution of damage events close to the failure. The distribution tail reveals a cutoff induced by finite size effect.

The behaviors of the susceptibility χ (Fig. 6), the order parameters $1-\zeta$ and O (Fig. 7) as functions of Δ remain unchanged as p is increased. They still behave according to a power law without significant changes of the exponent that remains close to 0.5 as for the dry FBM. This indicates that there is no change in the nature of the transition toward the

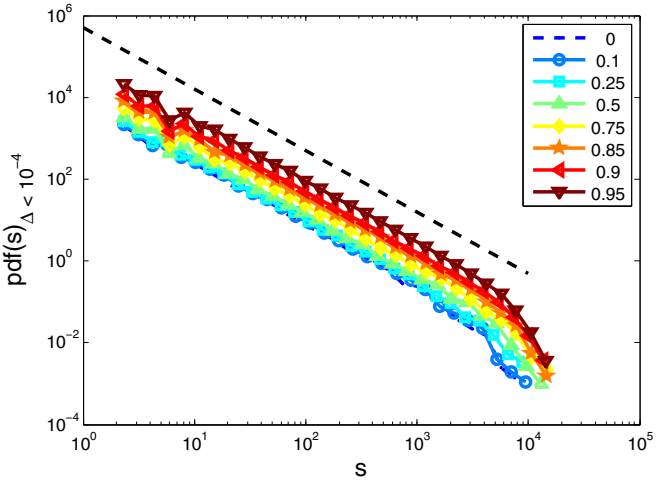

FIG. 5. Probability density function of the avalanche size, pdf(s), for fluid pressure p ranging from 0 to 0.95 (indicated in the legend) when $\Delta \to 0$ (i.e., $\Delta < 10^{-4}$). Dotted line corresponds to a power-law exponent of -1.5. The cutoff for largest sizes is a finite size effect.

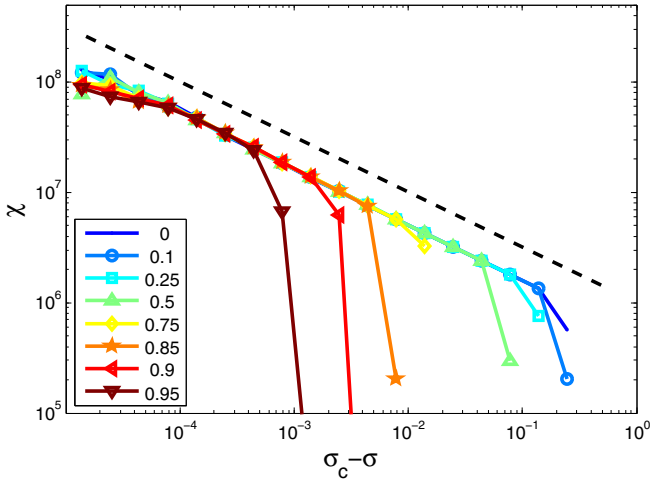

FIG. 6. Rate of size event χ as a function of the control parameter Δ, for simulations performed with pressure p varying from 0 to 0.95 (indicated in the legend). Dotted line corresponds to a power-law exponent of -0.5.

failure that can be considered to be continuous even for large values of p. Only the range of definition of the power law is reduced due to the decrease of σ_c as p is increased. That reduces our ability to forecast the failure.

IV. DISCUSSION

As mentioned previously, the aim of our work is to investigate the role played by the fluid pressure on the failure of heterogeneous brittle materials. In the model developed here, the behavior of the dry FBM is fully recovered for $p = 0$.

When accounting for the fluid pressure (i.e., for $p > 0$), the macroscopic behavior σ versus ϵ is kept unchanged in terms of shape. This is not surprising since the modification made to the model does not affect the rheology of the fibers. At the macroscopic scale, accounting for the fluid pressure thus results in a reduction of the maximal external load supported by the bundle. Both stress and strain values at the macrofailure decrease. This reduction is well accounted by the scaling factors $(1 - p)$ for strain and $(1 - p)^2$ for the stress, established analytically and well verified numerically (Fig. 2). As the fiber strength is spread at random from uniform distribution between 0 and 1, the value $p = 1$ appears as a peculiar point where even the critical load vanished. In such a case, the pressure applied on broken fibers is larger than the maximal fiber strength, so the failure is highly unstable and any avalanche may involve the whole set of fibers.

Below the limit of $p = 1$, the behavior of the FBMP toward the failure still conforms to a continuous transition as the order parameters $1 - \zeta$ and O grow continuously when the critical load is approached.

Contrastingly, the statistical properties of rupture avalanches are considerably affected by the modification made to the FBM. The power-law trend of the size probability density function, pdf(s), of the whole avalanche set is still observed but it is characterized by an exponent β decreasing from 2.5 for $p < 0.5$ to 1.5 when $p \to 1$ (Figs. 3 and 4). This could be simply explained by the narrowing of the stress range, when p is increased: as the maximal stress decreases, the system comes closer to criticality. But, considering that the change in β is not exactly correlated with the narrowing of the stress range (the decrease of β occurs essentially for $p > 0.75$, whereas σ_c decreases continuously with the increase of p), the stress range narrowing may not be the only explanation.

This loss of precursory behavior may be interpreted qualitatively as following: the force resulting from the fluid pressure applied on the damaged area increases as the number of broken fibers increases. Thus, during an avalanche, the number of remaining fibers decreases whereas the amount of load that the bundle have to support increases, even if the external load is kept constant. This is likely to induce larger avalanches compared with the dry FBM, and instabilities that may lead to macrofailure more rapidly. The abruptness of the transition to macrofailure increases with the fluid pressure. When considering avalanches occurring close to the macrofailure (Fig. 5), the pdf$(s)_{\Delta\to 0}$ reveals no change and shows a power-law trend with an exponent of $\tau = -1.5$, without any effect of p.

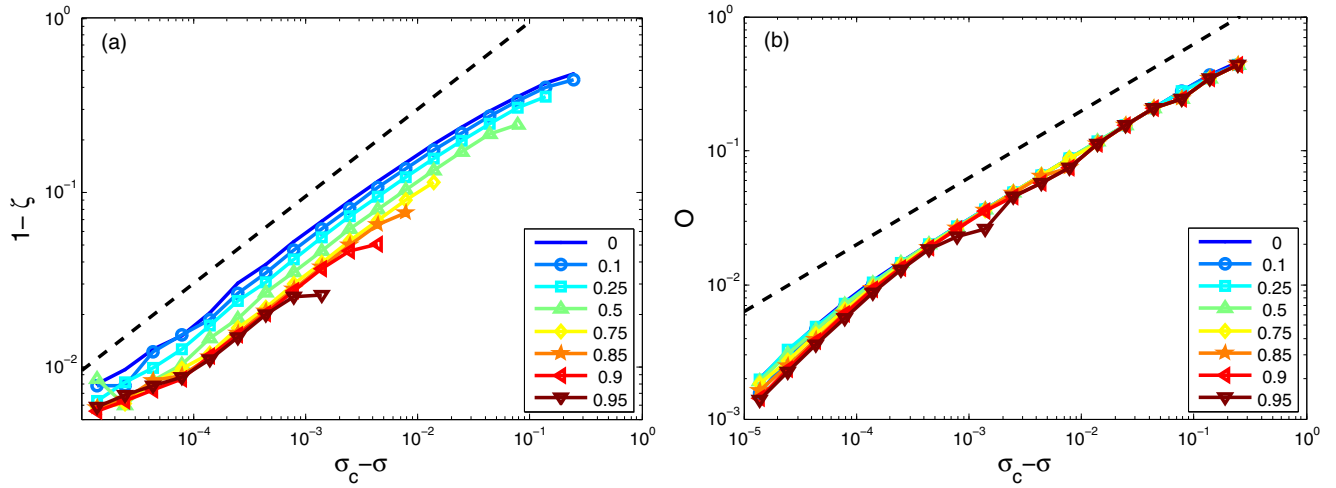

FIG. 7. Order parameters $1 - \zeta$ (a) and $O = U(\sigma_c) - U(\sigma)$ (b) against the control parameter $\Delta = \sigma_C - \sigma$ for simulations performed with pressure p varying from 0 to 0.95 (indicated in the legend). Dotted line corresponds to a power-law exponent of 0.5.

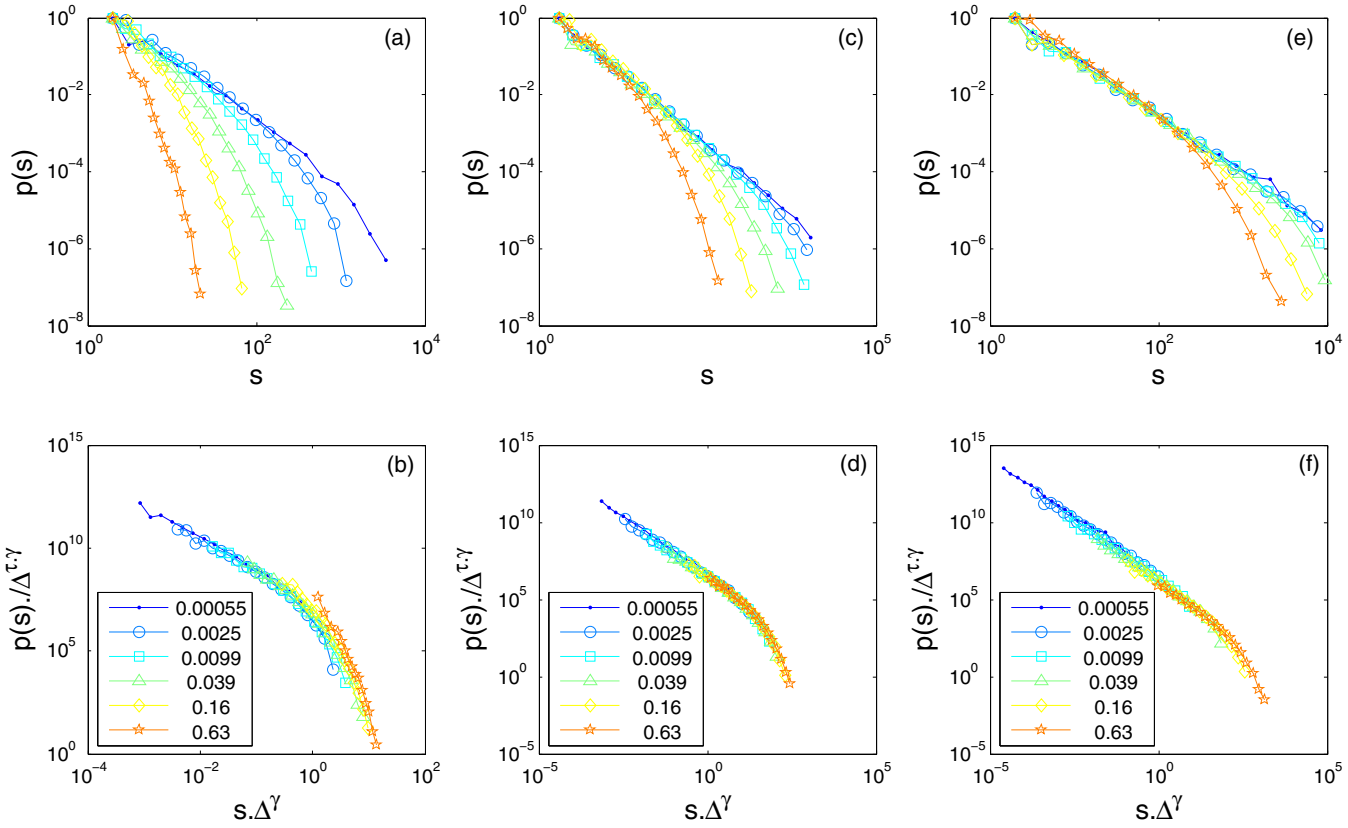

FIG. 8. Evolution of the avalanches size distribution as a function of the distance to macrofailure, for different values of the fluid pressure, $p = 0$ (a, b), $p = 0.75$ (c, d), and $p = 0.9$ (e, f). The Panels (a), (c), and (e) display the avalanches size distribution at different Δ values for $p = 0$ (a), $p = 0.75$ (c), $p = 0.9$ (e). Panels (b), (d), and (f) display the collapse of the avalanches size distribution according to Eqs. (19) and (20) for $p = 0$ (b), $p = 0.75$ (c), and $p = 0.9$ (e). The exponents β and τ are obtained from the fit of distributions shown in Figs. 3 and 5. The exponent γ is calculated according to Eq. (21). The legend indicates the Δ value corresponding to each distribution.

We analyze now the evolution of the avalanche size distribution as the macrofailure is approached and the relationship between τ and β. Figure 8 (top) shows the $\mathrm{pdf}(s,\Delta)$ for different ranges of Δ and different values of p (0, 0.5, and 0.9). The $\mathrm{pdf}(s,\Delta)$ can be described as a power law affected by a cutoff whose size diverges when $\Delta \to 0$. The distribution is well represented by a power law associated with an exponential tail that diverges as the control parameter Δ decreases, i.e., as the failure is approached:

$$\mathrm{pdf}(s,\Delta) = s^{-\tau} \exp(s/s_0) \tag{19}$$

with

$$s_0 = \Delta^{-\gamma}. \tag{20}$$

The good collapse shown on Fig. 8 demonstrates the pertinence of this model for the FBMP even for pressure values close to 1.

Considering the mechanism of *sweeping of an instability* proposed by Sornette [15] the γ, τ, and β exponents should be related according to [16]

$$\beta = \tau + 1/\gamma. \tag{21}$$

In the case of dry FBM, considering the theoretical values of $\beta = 2.5$ and $\tau = 1.5$, the γ exponent should be 1. This is in good agreement with our numerical estimations.

For the FBMP, when p is increased, as τ remains constant and β decreases, γ is supposed to increase what is confirmed by the numerical estimate of β, τ, and γ for various values of p (see Table I). The increase of the γ exponent corresponds to a faster divergence of the cutoff size s_0, which confirms the destabilizing effect of the fluid pressure.

TABLE I. Exponents characterizing the distribution of damage avalanches for p ranging from 0 to 1. β and τ are obtained by fitting the distributions shown in Figs. 3 and 5. γ is calculated using Eq. (21). These exponents are used for doing the collapse of the distributions for various values of p and Δ (Fig. 8).

Pressure	β ± 0.05	τ ± 0.05	γ $\pm 10\%$
0	2.50	1.50	1
0.1	2.50	1.50	1
0.25	2.50	1.50	1
0.5	2.50	1.50	1
0.75	2.45	1.50	1.05
0.85	2.10	1.50	1.65
0.9	1.80	1.50	3.3
0.95	1.55	1.50	>20

As a summary, for $p < 0.75$ the exponents remain quasiunchanged. For larger values, when p becomes close to 1, i.e., comparable with the largest fiber strength, there is a considerable decrease of β, which is well accounted in the model of sweeping of an instability by an abrupt increase of the γ exponent.

V. CONCLUSIONS AND PERSPECTIVES

Fluid pressure acts as destabilizing agent for the FBM. The interplay between damage and Biot's coefficient, that is explicitly taken into account in our model, modifies the progressive failure dynamics. The usual observations (power-law distribution of damage event, failure precursory behavior, divergence toward the failure) related to the behavior of brittle heterogeneous material during progressive rupture are still present as long as the fluid pressure remains not too large compared with the fiber strength. As the order parameter continuously grows toward critical load, the macrofailure can still be regarded as a second order transition, even for large pressure values. The exponents characterizing the behavior toward the failure are changed and the progressive acceleration of damage becomes more abrupt when fluid pressure is sufficiently increased. This reduces the ability to predict the failure. From the practical point of view, this highlights the importance of internal loading in addition to the external loading. The consequences for the predictability of failure in the presence of fluid pressure are of major importance.

According to our numerical results, when the ratio of fluid pressure to material strength remains close to zero, the usual behavior of the FBM is recovered with small changes of the characteristic exponents. This could correspond to natural conditions where the fluid pressure remains limited compared with material strength, e.g., hydrostatic water pressure compared with lithostatic stress. On the contrary, large values of fluid pressure, e.g., used for hydrofracturing, that are in the range of material strength may lead to uncontrolled failure as experienced in the geothermal site of Basel, Switzerland [17]. In such a case our results show the need for taking into account the increase of Biot's coefficient during the progressive damage process, which enhances the instability, whereas many studies considered this parameter to be constant [18].

We pointed out the considerable consequences that the fluid pressure can cause on material failure based on a modification of a simple lattice model, the FBM. It now appears crucial to pursue the work initiated in this study by accounting for more realistic scenarios: (1) where fluid flow is induced by pressure gradients within a porous media, (2) by considering heterogenous loading and local shear rules in two-dimensional geometry [19], and (3) by considering a continuous material and compressive stress states instead of pure tension. This will allow us to test the applicability to natural systems where compression is typically the dominant loading mode.

ACKNOWLEDGMENTS

The authors warmly thank anonymous reviewers for their constructive and detailed remarks and suggestions that helped us to strongly improve the manuscript. ISTerre is part of Labex OSUG@2020 (ANR10 LABX56).

[1] H. K. Gupta, A review of recent studies of triggered earthquakes by artificial water reservoirs with special emphasis on earthquakes in Koyna, India, Earth Sci. Rev. **58**, 279 (2002).
[2] R. M. Iverson, Landslide triggering by rain infiltration, Water Resour. Res. **36**, 18971910 (2000).
[3] Y. Guglielmi, F. Cappa, and D. Amitrano, High-definition analysis of fluid-induced seismicity related to the mesoscale hydromechanical properties of a fault zone, Geophys. Res. Lett. **35**, L06306 (2008).
[4] M. A. Biot, General theory of three-dimensional consolidation, J. Appl. Phys. **12**, 155 (1941).
[5] M. Kachanov, Elastic solids with many cracks and related problems, Adv. Appl. Mech. **30**, 259 (1994).
[6] K. Terzaghi, *Theoretical Soil Mechanics* (John Wiley, New York, 1943).
[7] F. Kun, S. Zapperi, and H. Herrmann, Damage in fiber bundle models, Eur. Phy. J. B **17**, 269 (2000).
[8] S. Zapperi, P. Ray, H. E. Stanley, and A. Vespignani, First-order Transition in the Breakdown of Disordered Media, Phys. Rev. Lett. **78**, 1408 (1997).
[9] M. J. Alava, P. K. Nukala, and S. Zapperi, Statistical models of fracture, Adv. Phys. **55**, (349) (2006).
[10] S. Pradhan and B. K. Chakrabarti, Failure properties of fiber bundle models, Int. J. Mod. Phys. B **17**, 5565 (2003).
[11] S. Pradhan, A. Hansen, and B. K. Chakrabarti, Failure processes in elastic fiber bundles, Rev. Mod. Phys. **82**, 499 (2010).
[12] S. Pradhan, P. Bhattacharyya, and B. K. Chakrabarti, Dynamic critical behavior of failure and plastic deformation in the random fiber bundle model, Phys. Rev. E **66**, 016116 (2002).
[13] Y. Moreno, J. B. Gomez, and A. F. Pacheco, Phase transitions in load transfer models of fracture, Physica A **296**, 9 (2001).
[14] G. Caldarelli, C. Castellano, and A. Petri, Criticality in models for fracture in disordered media, Physica A **270**, 15 (1999).
[15] D. Sornette, Sweeping of an instability: an alternative to self-organized criticality to get power laws without parameter tuning, J. Phys. I **4**, 209 (1994).
[16] D. Amitrano, Variability in the power-law distributions of rupture events, how and why does b-value change, Eur. Phys. J. Special Topics **205**, 199 (2012).
[17] M. O. Hring, U. Schanz, F. Ladner, and B. C. Dyer, Characterisation of the basel 1 enhanced geothermal system, Geothermics **37**, 469 (2008).
[18] J. Rutqvist and O. Stephansson, The role of hydromechanical coupling in fractured rock engineering, Hydrogeol. J. **11**, 7 (2003).
[19] S. Biswas and B. K. Chakrabarti, Crossover behaviors in one and two dimensional heterogeneous load sharing fiber bundle models, Eur. Phys. J. B **86**, 1 (2013).